RSC Advances

ROYAL SOCIETY OF CHEMISTRY

www.rsc.org/advances

RSC Advances

Paper

Mesoporous silica supported bimetallic Pd/Fe for enhanced dechlorination of tetrachloroethylene

Received 00th January 20xx,
Accepted 00th January 20xx

DOI: 10.1039/x0xx00000x

www.rsc.org/

Ruey-an Doong[a, b*], Sandip Saha[a], Cheng-Hsen Lee[b] and Hong-ping Lee[c]

In this study, the mesoporous silica (SiO_2) microspheres were hydrothermally synthesized in the presence of gelatin for immobilization of bimetallic Pd/Fe nanoparticles (Pd-Fe/SiO_2) to enhance the dechlorination efficiency and rate of tetrachloroethylene (PCE) under anoxic conditions. Scanning electron microscopy images and elemental mapping showed that the distribution of nanoscale zerovalent iron (NZVI, Fe) on SiO_2 was uniform and the density of Fe increased as the iron loading increased from 10 to 50 wt%. The optimized 30 wt% Fe/SiO_2 particles were used to fabricate Pd-Fe/SiO_2 microspheres by elctrochemical reduction of Pd ions to Pd^0 for the enhanced dechlorination of PCE under anoxic conditions. The dehlorination efficiency and rate of PCE by Fe/SiO_2 was significantly enhanced in the presence of 0.5–3 wt% Pd and the pseudo-first-order rate constant (k_{obs}) for PCE dechlorination by mesoporous Pd-Fe/SiO_2 microspheres increased 2–3 orders of magnitude when compared with that of Fe/SiO_2 alone. Ethane was found as the only end product with the carbon mass balance of 95–100%, showing that hydrodechlorination was the main reaction mechanism for PCE dechlorination by Pd-Fe/SiO_2 microspheres. Column experiments showed the good mobility and permeability of mesoporous Pd-Fe/SiO_2 micrsopheres compared with that of pure NZVI alone. Results obtained in this study clearly show that the immobilization of bimetallic Pd-Fe nanoparticles on the mesoporous SiO_2 microspheres not only increases the reactivity for dechlorination of PCE but also enhances the mobility and permeability for in-situ remediation of chlorinated hydrocarbons in porous media.

1. Introduction

The contamination of porous media such as soils and groundwater by dense non-aqueous phase liquids (DNAPLs) is becoming a serious environmental issue. DNAPLs such as tetrachloroethylene (PCE) and trichloroethylene (TCE) have been extensively used as cleaning solvents, aerosol propellants and refrigerants, and are released into the aquatic environments as the priority pollutants in both surface water and groundwater.[1-3] These chemicals are possible carcinogens which pose a serious health concern to human beings because of their toxic and mutagenic behaviours.[4, 5] Therefore, an urgent need in the development of effective strategy for removal of chlorinated hydrocarbons in the contaminated aquifers is required.

Several technologies have been developed for the detection[6] and dechlorination of chlorinated hydrocarbons.[7-10] Permeable reactive barriers (PRBs) packed with zerovalent metals has been demonstrated to be an effective method for the removal of organic and inorganic pollutants under anoxic conditions.[11-13] Various laboratory-scale and field applications have found that nanoscale zerovalent iron (NZVI) and bimetallic iron-based nanoparticles including Fe/Pd and Fe/Ni can transform the chlorinated compounds into less-chlorinated homologues and non-chlorinated end products through the reductive dechlorination and hydrodechlorination.[14-18] Several studies have depicted that chlorinated hydrocarbons can be rapidly dechlorinated into non-chlorinated hydrocarbons by using nanoscale bimetallic Pd/Fe particles.[18,19] However, the aggregation of NZVI decreases the dechlorination efficiency and rate of chlorinated compounds. Several studies have demonstrated the effectiveness of using stabilizer or support to homogeneously disperse NZVI nanoparticles to enhance their stability and mobility.[20-28] Various organic polymers including carboxymethyl cellulose, polyacrylic acid (PAA) and electrospun PAA/polyvinyl alcohol nanofibers have been used to immobilized Pd/Fe for the enhanced dechlorination efficiency and rate of chlorinated compounds.[22, 23] In addition, the organic polymer-immobilized iron-based nanoparticles have high mobility to facilitate the nanoparticle transport through soil columns.[24, 25]

Another strategy for the increase in stability and reactivity of nanoparticles is the immobilization on supports such as membranes and carbon materials.[26-31] Parshetti and Doong[28] have immobilized

[a] Institute of Environmental Engineering, National Chiao Tung University, Hsinchu, 30010, Taiwan. E-mail: radoong@nctu.edu.tw
[b] Department of Biomedical Engineering and Environmental Sciences, National Tsing Hua University, Hsinchu, 30013, Taiwan.
[c] Department of Chemistry, National Cheng Kung University, Tainan, 700, Taiwan.

†Electronic Supplementary Information (ESI) available: TEM images and surface areas of mesoporous SiO_2; XRD patterns, adsorption and dechlorination of PCE by Fe/SiO_2; TEM images, deconvolution of XPS spectra and column experiments of Pd-Fe/SiO_2]. See DOI: 10.1039/x0xx00000x

bimetallic Ni/Fe nanoparticles in PVDF and nylon 66 membranes in the presence of polyethylene glycol for dechlorination of TCE and found that the immobilization of Fe/Ni nanoparticles in the hydrophilic membrane can retain the longevity and high reactivity of nanoparticles towards TCE dechlorination. In addition, Su et al. used activated carbon-supported zerovalent iron (ZVI/AC) for adsorption and dechlorination of TCE.[27] The rate constant for TCE dechlorination by ZVI/AC was 7 times higher than that by AC only. More recently, silica has been used as the support to maintain the reactivity and stability of iron-based nanoparticles.[32-34] The use of mesoporous SiO_2 microspheres as the support have several advantages including the prevention of NZVI agglomeration, environmental friendliness and the increased reactivity and stability. Ensie and Samad have immobilized NZVI onto SiO_2@FeOOH core using reduction method to remove nitrate from drinking water and found that greater than 99% of nitrate could be removed by the nano SiO_2@FeOOH@Fe core-shell materials at pH 3.[34] In addition, Xie et al. have compared four different iron-based nanoparticles for dechlorination of polybrominated diphenyl ethers.[32] Results showed that the core-shell type SiO_2@FeOOH@Fe materials had higher usability and stability and low leaching Fe^{2+} rate compared to the other iron-based materials. It is noteworthy that mesoporous SiO_2 microsphere is stable, environmentally friendly and can be transported with water in porous media. However, the use of mesoporous SiO_2 microspheres as the support for bimetallic Pd/Fe nanoparticles for dechlorination of chlorinated hydrocarbons has received less attention. In addition, little information is available on the characterization and dechlorination efficiency of bimetallic Pd-Fe nanoparticles on mesoporous silica.

In this work, the bimetallic Pd/Fe nanoparticles were immobilized onto mesoporous SiO_2 microspheres for PCE dechlorination under anoxic conditions. Mesoporous SiO_2 microspheres were hydrothermally fabricated in the presence of gelatin and then the bimetallic Pd/Fe nanoparticles were immobilized onto the surface of mesoporous SiO_2. The microstructures of Pd-Fe/SiO_2 microspheres including morphology, specific surface area, pore textuture, and chemical species were characterized. The effect of Fe and Pd loadings on the dechlorination efficiency and rate of PCE were optimized. In addition, the longevity and stability of mesoporus Pd-Fe/SiO_2 microspheres were investigated.

2. Materials and methods

2.1 Reagents

Chlorinated hydrocarbons including PCE and TCE (99.8%, GC grade) used in this study were purchased from Merck Co. (Darmstadt, Germany). Palladium acetate ($Pd(CH_3CO_2)_2$, 98 %) was obtained from Fluka Co. (Tokyo, Japan). HEPES (N-[2-hydroxyethyl] piperazine-N'-[2-ethanesulfonic acid]) ($C_8H_{18}N_2O_4S$) and ferrous sulfate-7-hydrate ($FeSO_4{\cdot}7H_2O$) were purchased from Sigma Co. (St. Louis, MI). All other reagents were of analytical grade and were used as received without further treatment. In addition, the deoxygenated water was prepared by vacuuming the well-mixed deionized bidistilled water (18.3 MΩ cm, Millipore Co.) in serum bottles for 20 min and then purged with nitrogen for 5.0 min at 12.5 psi. The above procedure was repeated several times to remove oxygen in solutions.[9]

2.2. Synthesis of mesoporous silica

The stock solution of silicate was obtained upon mixing 20 g of sodium silicate, 250 mL of deionized bidistilled water and 250 mL of 0.1 M H_2SO_4 solution at 40 °C. The final pH of solutions was then adjusted to 5. The fresh gelatine solution, prepared by adding 10 g of gelatin into 125 mL of water at 40 °C, was poured directly to the acidic solution of sodium silicate and stirred for several minutes. Solutions were hydrothermally treated at 100 °C for 1 d to form mesoporous silica. After cooling down to room temperature, products were harvested by filtration, washed with water, dried in air and calcined at 550 °C.

2.3. Immobilization of Pd-Fe nanoparticles onto mesoporous silica

The Fe/SiO_2 was synthesized by dispersing 0.3 g of mesoporous silica microspheres in 100 mL of bidistilled deionized water. 0.3 g of $FeSO_4{\cdot}7H_2O$ were added into the mesoporous SiO_2 solution and Fe/SiO_2 microspheres were synthesized by adding 50 mL of 0.2 M ice-bathed $NaBH_4$ solution dropwisely to reduce the ferrous ions into NZVI at pH 4 under stirring conditions. The mesoporous Fe/SiO_2 microspheres were collected by centrifugation at 14,000 rpm for 10 min and then dried in N_2. In addition, the bimetallic Pd-Fe/SiO_2 microspheres were fabricated using electrochemical reduction method by addition of deoxygenated 0.1−3 wt% $Pd(CH_3COO)_2$ solutions into the Fe/SiO_2 solutions under anoxic conditions. The Pd concentrations in Pd-Fe/SiO_2 microspheres were also examined by inductively coupled plasma-mass spectrometer (ICP-MS, Agilent 7500ce). The measured Pd concentrations were in the range of 0.095-2.86 wt%, which corresponded to the recovery of 94−97%.

$$Pd^{2+} + Fe^0 \rightarrow Pd^0 + Fe^{2+} \quad (1)$$

2.4. Dechlorination of PCE by Pd-Fe/SiO_2 microspheres

The dechlorination of PCE by mesoporous Pd-Fe/SiO_2 microspheres was performed by using batch experimental systems. N_2-purged serum bottles containing 0.1 g of Pd-Fe/SiO_2 or pure NZVI were filled with 50 mL of 25 mM HEPES buffer solutions at pH 7.2 in glove box. After being capped with Teflon-lined rubber septa and aluminium caps, stock solutions of PCE were introduced into the bottles to get the final concentration of 5 mg/L. Serum bottles were then incubated in an orbital shaker at 120 rpm and at 25 °C in the dark. Control experiments were also preformed in the absence of mesoporous Pd-Fe/SiO_2 microspheres.

Column experiments were performed by using a 15 mL glass burette packed with 0.4−0.6 mm glass beads to investigate the mobility and water permeability of Pd-Fe/SiO_2 microspheres and NZVI. The column diameter was 1.5 cm and the total pore volume was 11.9 cm^3. Columns were saturated with deoxygenated

deionized water before the addition of 2 g/L NZVI or Pd-Fe/SiO_2 suspensions. The flow rate of the feeding solution was 4.8 mL/min.

2.5. Analysis and characterization

The chlorinated as well as non-chlorinated hydrocarbons were determined by injecting 40 μL of headspace gas in the serum bottles into a Perkin-Elmer gas chromatograph (GC) equipped with an electron capture detector (ECD) and a flame ionization detector (FID). The VOCOL fused-silica megabore capillary column was used to separate the chlorinated and non-chlorinated compounds by isothermally maintaining at 120 °C using ultra high purity nitrogen (> 99.9995%) as the carrier gas. The temperatures of ECD and FID were maintained at 325 and 250 °C, respectively. Blank controls were also performed to examine the possible loss of chlorinated compounds during the dechlorination periods. In addition, aqueous concentrations of chlorinated hydrocarbons were calculated using the external standard method by preparing the known concentrations of chlorinated hydrocarbons in aqueous solutions.

The crystallite size and crystal phase of Pd-Fe/SiO_2 microspheres were examined by a Scintag X1 advanced X-ray diffractometer (XRD) with Ni-filtered Cu Kα radiation (λ= 0.1541 nm). The XRD patterns were obtained from 20° to 70° 2θ with the sampling step width of 0.05° and step time of 0.5 s. The specific surface area, pore volume and pore size distribution were determined by the N_2 adsorption-desorption isotherms at 77 K using a ASAP 2020 surface area and porosimetry system manufactured by Micromeritics Co. The Brunauer-Emmett-Teller (BET) method was utilized to calculate the specific surface areas (S_{BET}) using adsorption data in a relative pressure (P/P_0) range from 0.02 to 0.2. By using the Barrett-Joyner-Halenda (BJH) model, the pore volumes and pore size distributions in the mesopore range (> 2 nm) could be derived from the adsorption branches of the isotherms, and the total pore volumes (V_t) were calculated from the adsorbed amount at a relative pressure of 0.995.

The surface morphology of mesoporous Pd-Fe/SiO_2 microspheres was observed using JOEL field-emission scanning electron microscope (FE-SEM). The TEM images and particle sizes of Pd-Fe/SiO_2 were obtained from a Hitachi H-7500 transmission electron microscopy at an acceleration voltage of 80 kV by suspending one drop of microsphere suspension on a 300-mesh carbon coated Cu grid. The X-ray photoelectron spectroscopic (XPS) measurements were performed by ESCA PHI 1600 photoelectron spectrometer using Al Kα X-ray source (1486.6 eV). The binding energies of the photoelectrons were determined by assuming that the carbon 1s electron has a binding energy of 284.8 eV. During the data acquisition, the pressure in the sample chamber did not exceed 2.5×10^{-9} Torr.

3. Results and discussion

3.1. Microstructures of Fe/SiO_2 microspheres

The morphology and specific surface area of mesoporous SiO_2 microspheres were first characterized. Fig. S1 (†ESI) shows the TEM images of mesoporous SiO_2 fabricated at various hydrothermal times ranging from 1 to 7 d. It is clear that the particle sizes of mesoporous SiO_2 increased with the increase in hydrothermal time and the particles diameters were in the range of 1–5 μm. In addition, the mesoporous silica showed typical type IV isotherms with hysteresis loop in the P/P_0 range of 0.5–0.95, clearly showing the mesoporous characteristics of SiO_2 (Fig. S2, †ESI). The specific surface area of mesoporous SiO_2 microspheres decreased from 312 m^2/g at 1 d to 164 m^2/g at 7 d, while the average pore diameter increased slightly from 6.9 to 8.6 nm when the hydrothermal time increased from 1 to 7 d. Since the role of mesoporous SiO_2 microspheres used in this study is to serve as the support, the hydrothermal time of 1 d was selected because of the high surface area and similar pore diameter for immobilization of NZVI.

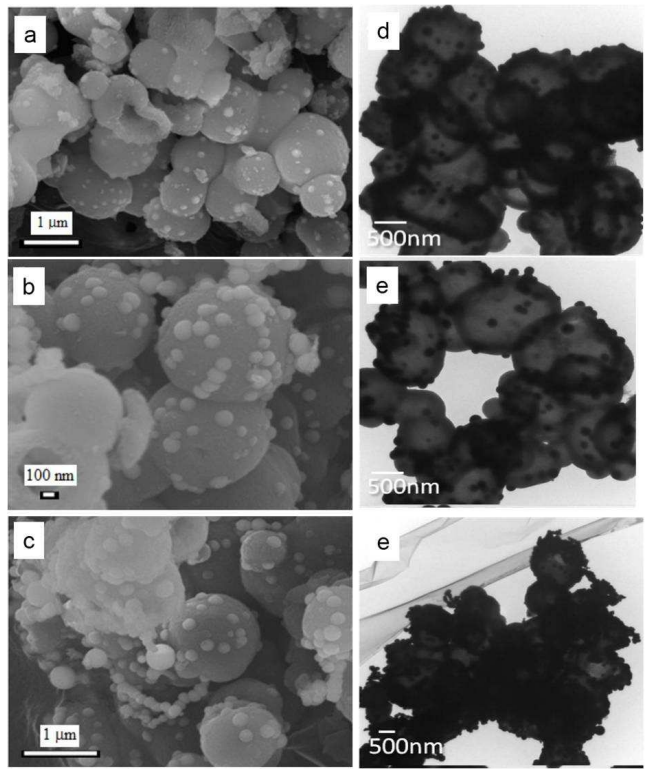

Fig. 1. The SEM and TEM image images of various iron loadings of Fe/SiO_2 microspheres. (a)-(c) SEM images of 10, 30, and 50 wt% Fe/SiO_2, (d)-(f) TEM image of 10, 30 and 50 wt% Fe/SiO_2.

Fig. 1 shows the SEM and TEM images of 10–50 wt% Fe/SiO_2 prepared by adding 50 mL of 0.2 M $NaBH_4$ into mesoporous SiO_2 solutions containing ferrous ions. It is clear that the particle numbers as well as sizes of NZVI onto SiO_2 microspheres increased with the increase in Fe loading. No obvious aggregation of NZVI was observed when the loading of Fe was lower than 30 wt% (Fig. 1(a) and 1(b)). However, the NZVI aggregated into large particles at 50 wt% Fe and some NZVI nanoparticles were agglomerated into the long chains outside the SiO_2 microspheres (Fig. 1(c)). The EDS analysis indicated that the atomic ratios of Fe to Si were 0.122 for

10 wt% Fe/SiO_2, 0.316 for 30 wt% Fe/SiO_2 and 0.575 for 50 wt% Fe/SiO_2. In addition, the ICP-MS analysis showed similar results and the Fe concentration was 12.5 wt% for 10 wt% Fe/SiO_2, 30.3 wt% for 30 wt% Fe/SiO_2, and 45.1 wt% for 50 wt% Fe/SiO_2. These results clearly indicate the nearly complete reduction of ferrous ions to NZVI on the surface of mesoporous SiO_2 by $NaBH_4$.

Similar to the SEM images, the TEM images clearly showed the formation of discrete NZVI nanoparticles onto the surface of mesoporous SiO_2 microspheres when the Fe loadings were in the range 10–30 wt% (Fig. 1(d) and 1(e)). In contrast, the agglomeration of long-chained NZVI was clearly observed at 50 wt% Fe/SiO_2 (Fig. 1(f)). Fig. 2 shows the histogram of particle sizes of NZVI onto Fe/SiO_2 at various iron loadings of 10–50 wt%. The particle size distributions of NZVI at 10 wt% Fe/SiO_2 were in the range of 60-160 nm, and then increased to 120–240 nm at 50 wt% Fe/SiO_2. In addition, the average particle sizes of NZVI were 85 ± 27 nm, 150 ± 21 nm and 165 ± 30 nm for 10, 30, and 50 wt% Fe/SiO_2, respectively. No obvious difference in mean diameter of NZVI between 30 and 50 wt% Fe/SiO_2 reflected the fact that 30 wt% could be the optimal iron loading for mesoporous SiO_2 microspheres.

Fig. 3 shows the XRD patterns and specific surface areas of Fe/SiO_2 microspheres with various Fe loading. As shown in Fig. 3a, the XRD patterns of pure NZVI showed peaks centered at 44.6° and 65.0° 2θ, which can be assigned as (110) and (200) planes of body-centered cubic Fe (JCPDS 06-0696) respectively.[35] The broad peak at 20–25° 2θ of Fe/SiO_2 microspheres was mainly attributed from the amorphous characteristics of SiO_2. In addition, the small and broad peak at 44.6° 2θ appeared when the iron loading increased from 10 to 50 wt%, indicating the successful immobilization of NZVI onto the surface of SiO_2.

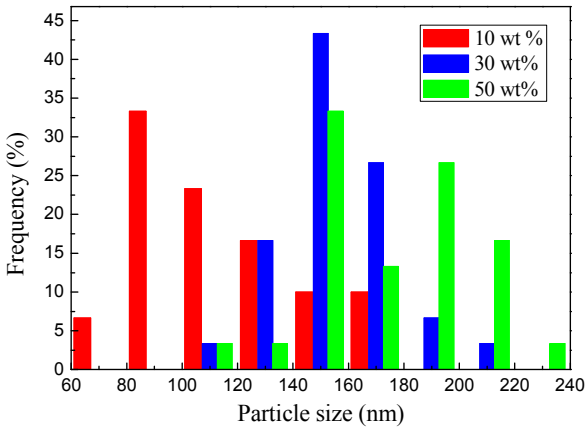

Fig. 2. The particle size distribution of NZVI onto Fe/SiO_2 microspheres at various iron loadings ranging from 10 to 50 wt%.

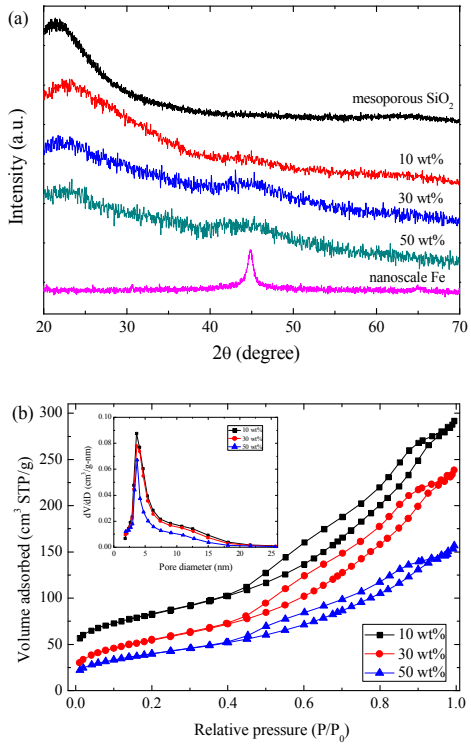

Fig. 3. The (a) XRD patterns and (b) N_2 adsorption-desorption isotherms of 10–50 wt% Fe/SiO_2. The insert in Fig. (b) is the pore size distribution of Fe/SiO_2. The y-axis of 10 wt% Fe/SiO_2 was vertically shifted for 25 cm^3/g for clarity.

Fig. 3b shows the BET surface area of 10–50 wt% Fe/SiO_2 microspheres. Similar to the pure mesoporous SiO_2 microspheres, the N_2 adsorption-desorption isotherms of Fe/SiO_2 with various Fe loadings followed type IV physisorption isotherm with H3 hysteresis loop in the P/P_0 range of 0.4–0.95, which is mainly attributed to the capillary condensation in the mesopores of silica substrate.[36] The specific surface areas of 10 and 30 wt% Fe/SiO_2 were in the range of 196–209 m^2/g and then decreased to 143 m^2/g when the Fe loading increased to 50 wt%. In addition, the pore size distributions of 10–50 wt% Fe/SiO_2 were similar and the average pore diameters were in the range 5.7–6.0 nm, which indicate that the decrease in specific surface area of 50 wt% Fe/SiO_2 is mainly attributed to the formation of large and excess NZVI nanoparticles onto and outside the mesoporous SiO_2 microspheres. It is noteworthy that the average pore diameter of Fe/SiO_2 microspheres is smaller than that of pure SiO_2 microspheres, presumably attributed the formation of NZVI onto the surface of SiO_2 microspheres.

3.2 Microstructures of Pd-Fe/SiO_2 nanoparticles.

After the successful fabrication of Fe/SiO_2, Pd precursor was added into the Fe/SiO_2 to electrochemically formation of bimetallic Pd-Fe nanoparticles onto mesoporous SiO_2 microspheres. 30 wt% Fe/SiO_2 microspheres were selected as the supports because of the homogenous Fe nanoparticles on SiO_2 surface and large specific

surface area. Fig. S3 (†ESI) shows the XRD patters of 0.5–3 wt% Pd-Fe nanoparticles onto mesoporous SiO_2 microspheres. The XRD patterns of various Pd loadings of Pd-Fe/SiO_2 microspheres showed broad peaks at 20-25° 2θ, which were similar to the results obtained by Fe/SiO_2 microspheres. No Fe peaks at 44.6° 2θ was observed, presumably attributed to the transformation of NZVI into iron oxides by providing electrons to electrochemically reduce Pd^{2+} into Pd^0. The TEM images of 1–3 wt% Pd-Fe/SiO_2 microspheres clearly showed the formation of thin layer on the surface of NZVI with some needle-like structures (Fig S4, †ESI), indicating the formation of iron oxides after the addition of Pd ions. However, no characteristic Pd peak was observed because of the low added amounts of Pd onto Fe/SiO_2.

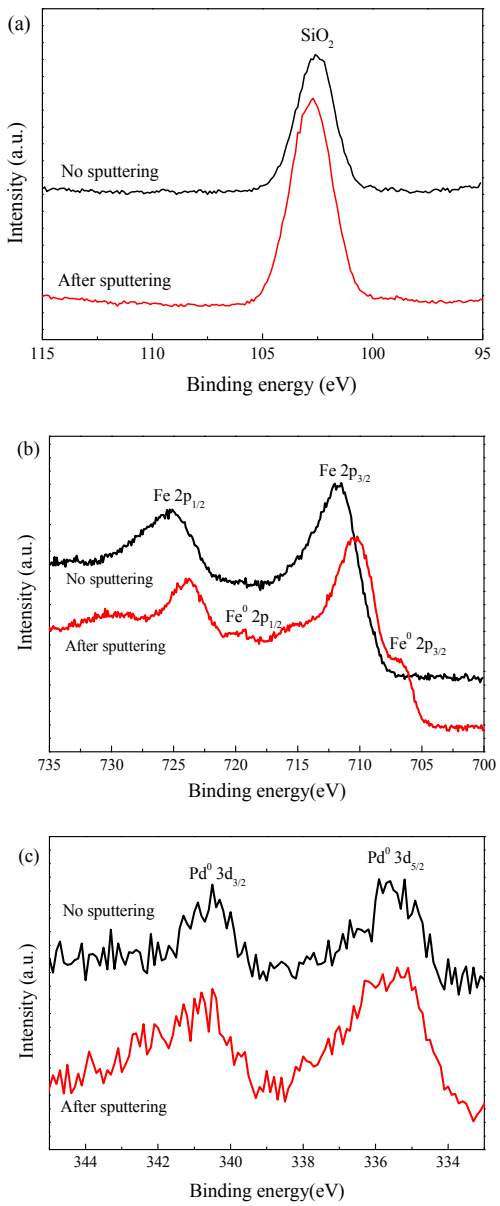

Fig. 4. The XPS spectra at (a) Si 2p, (b) Fe 2p and (c) Pd 3d of 3 wt% Pd-Fe/SiO_2 microspheres.

To further elucidate the immobilization of Pd onto Fe/SiO_2 surfaces, XPS was used to characterize the change in chemical species of elements in Pd-Fe/SiO_2 microspheres. Fig. 3 shows the XPS spectra of Si 2p, Fe 2p and Pd 3d species in 3 wt% Pd-Fe/SiO_2 microspheres. The XP spectrum of Si 2p showed a broad peak at 100-105 eV, indicating the formation of SiO_2 (Fig. 3a). After Ar sputtering for 1 min to remove top 27 nm of the particle surfaces, the Si 2p peak still remained at the same position, indicating the stability of SiO_2 as the support. The XPS of Fe 2p showed two peaks centered at 711 and 724 eV, which were the characteristic Fe $2p_{3/2}$ and Fe $2p_{1/2}$ peaks of iron oxides (Fig. 3b). Additional zerovalent iron peaks at 707 and 720 eV appeared after Ar sputtering for 1 min, clearly indicating the transformation of ZNVI to iron oxides after addition of Pd^{2+}. This result also supports the XRD results that no iron species was identified in Pd-Fe/SiO_2 microspheres. In addition, the XPS peaks of iron oxides shifted from 711.8 eV to 710.4 eV. After peak deconvolution, the major species of iron oxides changed from goethite (FeOOH) to magnetite (Fe_3O_4) after Ar sputtering (Fig S5, †ESI), which reflect the fact that the reduction of Pd^{2+} to Pd^0 changed the species of iron oxides on the surface of NZVI. The XPS spectra of 3 wt% Pd loaded Fe/SiO_2 showed Pd 3d peaks at 334.9 and 340.2 eV, which belonged to Pd^0 $3d_{5/2}$ and Pd^0 $3d_{3/2}$ peaks, respectively (Fig. 3c). The peak position of Pd species did not change after Ar sputtering for 1 min, clearly indicating the formation of zerovalent Pd. In addition, no other peak related to oxidation state of Pd^{2+} was observed, confirming the complete reduction of immobilized Pd^{2+} to Pd^0 through the electrochemical Pd^{2+}–Fe^0 reduction reaction.

3.3. Dechlorination of PCE by Pd-Fe/SiO_2 microspheres

Since the SiO_2 microspheres are mesoporous materials and could adsorb organic contaminants, the adsorption experiment of PCE by mesoporous SiO_2 microspheres was examined first. Fig. S6 (†ESI) shows the adsorption of 5 mg/L PCE onto mesoporous SiO_2 microspheres. No obvious decrease in PCE concentration was observed after 50 h of incubation, indicating that the adsorption of PCE onto mesoporous SiO_2 microspheres can be neglected. In addition, the dechlorination efficiency of PCE by pure NZVI and Fe/SiO_2 was compared at pH 5.5. As shown in Fig. S7 (†ESI), the dechlorination efficiency of PCE by Fe/SiO_2 after 575 h of incubation was higher than that of pure NZVI. The dechlorination followed the pseudo-first-order rate kinetics and the pseudo-first-order rate constants (k_{obs}) for PCE dechlorination were 0.0061 and 0.0042 h^{-1} for Fe/SiO_2 microspheres and pure NZVI, respectively. Since SiO_2 has no reactivity on PCE dechlorination, the dechlorination of PCE is mainly contributed from the NZVI onto SiO_2 microspheres and the rate constant for PCE dechlorination can be normalized to the unit mass of NZVI to reflect the reactivity of NZVI onto Fe/SiO_2. After normalization to the unit mass of NZVI, The mass-normalized rate constant (k_m) for PCE dechlorination by Fe/SiO_2 was 0.01 L/h-g. This value is 4.8 times higher than that by pure NZVI, presumably attributed to the well-dispersed NZVI on the surface of SiO_2 microspheres.

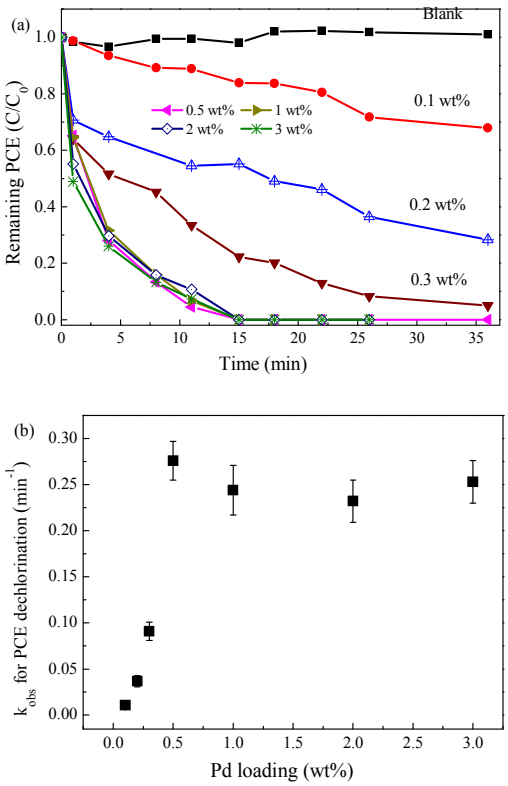

Fig. 5. The (a) dechlorination of PCE by 0.1–3 wt% Pd-Fe/SiO_2 under anoxic conditions and (b) pseudo-first-order rate constant for PCE dechlorination as a function of Pd loading.

Addition of second catalytic metal ions such as Pd, Ni and Pt onto the iron surface can significantly enhance the dechlorination rate and efficiency of chlorinated compounds.[35, 37, 38] Fig. 5a shows the dechlorination efficiency of PCE by SiO_2-supported Pd-Fe nanoparticles at various Pd loadings of 0.1–3 wt%. The dechlorination efficiency of PCE by Pd-Fe/SiO_2 increased significantly from 33% at 0.1 wt% Pd to 99.5% at 0.3 wt% Pd and a nearly complete PCE dechlorination was observed at Pd loading > 0.5 wt%. Fig. 5b shows the k_{obs} for PCE dechlorination as a function of Pd loading. The k_{obs} values increased positively from 0.011 ± 0.004 min^{-1} at 0.1 wt% Pd to 0.267 ± 0.021 min^{-1} at 0.5 wt% Pd and then slightly decreased to 0.253 ± 0.023 min^{-1} when Pd concentration increased to 3 wt%. These values are 2–3 orders of magnitude (108–2,625 times) higher than that of pure Fe/SiO_2 microspheres at pH 5.5, showing that addition of low amounts of Pd ions can significantly enhance the dechlorination efficiency and rate of PCE by mesoporous SiO_2-supported NZVI.

Several studies have addressed the effect of additive loadings on the dechlorination efficiency of chlorinated hydrocarbons by zerovalent metals.[39-41] An optimal mass loading often exists for a wide variety of bimetallic catalysts including Ni/Fe, Pd/Fe, Ni/Si and Ru/Fe. Lin et al. reported that the dechlorination rate of TCE by bimetallic Ru/Fe increased as the Ru loading increased from 0.25 to 1.5 wt%.[41] A decrease in k_{obs} was also observed when Ru loading increased to 2.0 wt%. In this study, an optimal dosage of 0.5 wt% Pd ions was obtained for the dechlorination of PCE by Fe/SiO_2 microspheres. The addition of catalytic Pd ions prevents the formation of toxic products by dechlorination of chlorinated hydrocarbons via hydrogen reduction rather than through electron transfer.[35] As shown in Fig. 6, ethane was the only detected products for dechlorination of PCE by 0.5–3 wt% Pd-Fe/SiO_2 and the carbon mass balances were all greater than 95%, showing that hydrodechlorination is the major reaction mechanism for dechlorination of PCE by mesoporous Pd-Fe/SiO_2 microspheres. In addition, several studies have reported the hydrodechlorination of gaseous PCE over Pd-based catalysts in the presence of hydrogen under high temperature conditions.[42-44] Bueres et al. immobilized 1 wt% Pd catalysts on three different carbonaceous materials and found that 68-97% of gaseous PCE were converted to ethane and trace amounts of TCE by carbon supported Pd at 525 K after 30 h of incubation.[44] This indicates that Pd only can show its dechlorination ability at high temperature and Pd-Fe/SiO_2 microspheres are excellent catalysts for hydrodechlorination of PCE in aqueous solutions.

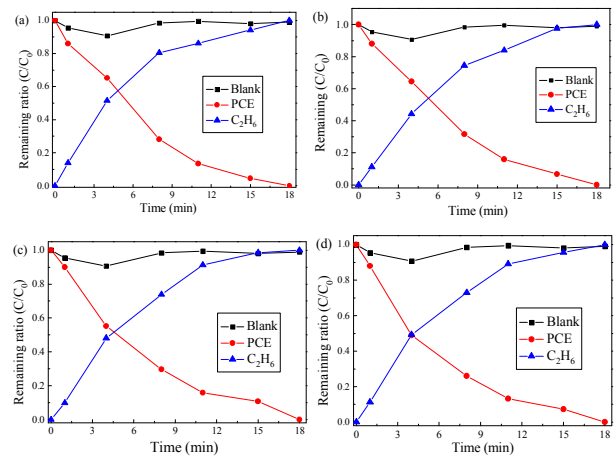

Fig. 6. The production of ethane and carbon mass balance during the dechlorination of PCE by various Pd loadings of Pd-Fe/SiO_2 microspheres. (a) 0.5, (b) 1, (c) 2 and (d) 3 wt% Pd.

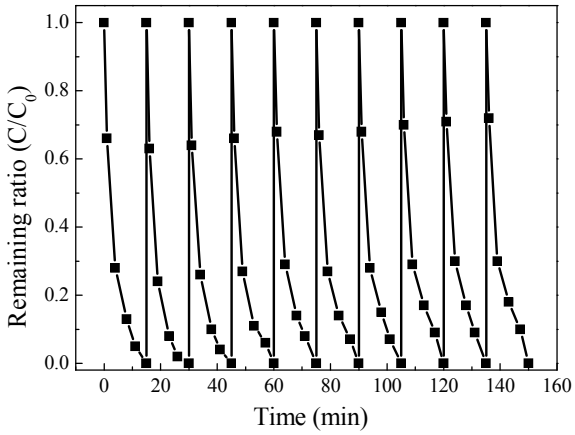

Fig. 7. The stability and longevity of mesoporous Pd-Fe/SiO_2 microspheres with repeated spiking of 5 mg/L PCE.

The long-term performance of 0.5 wt% Pd-Fe/SiO_2 on the dechlorination of PCE was further investigated by repeatedly injected of 5 mg/L PCE into the solutions containing Pd-Fe/SiO_2 microspheres. Fig. 7 shows the stability and longevity of Pd-Fe/SiO_2 with the repeated spiking of PCE under anoxic conditions. A fast PCE dechlorination process was observed and the Pd-Fe/SiO_2 microspheres can be reused for at least 10 times with stable dechlorination efficiency of all > 99%. Several studies have reported the repeated use of Pd/Fe nanoparticles for dechlorination. Nagpal et al. have used bimetallic Fe–Pd nanoparticles for lindane degradation under anoxic conditions and found that the dechlorination efficiency of the recycled Fe–Pd dropped slightly to 92% after 10th cycle.[45] In this study, the k_{obs} values and initial rate for PCE dechlorination were in the range 0.207–0.271 min^{-1} and 8.96–11.5 μM/min, respectively, showing that 0.5 wt% Pd-Fe/SiO_2 microspheres are a promising material for dechlorination of chlorinated hydrocarbons. The stability of Pd-Fe/SiO_2 is mainly attributed to the introduction of SiO_2 as the support. Reardon et al. have proposed that the presence of silica may slow down the iron corrosion by adsorbing silicate, the dissolved form of SiO_2 after reaction, to the anodic surface.[46] In this study, the solution pH after dechlorination in the presence of Fe/SiO_2 microspheres increased 0.4–0.8 unit which is lower than that in the presence of pure NZVI (1–1.5 units). This result supports the hypothesis that the introduction of SiO_2 microspheres could maintain the reactivity of NZVI with > 99% dechlorination efficiency of PCE.

3.4. Column experiments

One of the advantages of using mesoporous SiO_2 microsphere as the support is the high mobility and water permeability during the dechlorination processes. To prove the merits of mesoporous SiO_2 microspheres, column experiments were conducted to understand the water permeability in the presence of Pd-Fe/SiO_2 microspheres. As shown in Fig. S8 (†ESI), the pure NZVI was retained on the top of the column, which was similar to those reported data.[22, 47] In contrast, the Pd-Fe/SiO_2 microspheres could transport along with the water through the whole column, which indicate the good transportability of Pd-Fe/SiO_2. Fig. 8 shows the breakthrough curves of pure NZVI and Pd-Fe/SiO_2. It is clear that mass ratios of pure NZVI in the effluent were in the range of 0.01-0.06 in the first 6 pore volumes, showing that NZVI would be aggregated into large particles and then retained in the column. On the contrary, the mass of Pd-Fe/SiO_2 microspheres in the effluent started to increase after 3 pore volumes and 90% of Pd-Fe/SiO_2 were eluted from the column after 6 pore volumes. Zhan et al. compared the mobility of Fe/ethylsilica and NZVI using a column packed with standard Ottawa sand and found that most NZVI was trapped within the first few centimeters of the column, while Fe/ethylsilica particles reached the column bottom[47], which is consistent with the results obtained in this study.

Fig. 8b shows water permeability of pure NZVI and Pd-Fe/SiO_2 by packing 1 cm of different materials in the middle of column. In the absence of Fe-based particles, the average water flow in the glass bead packed column was 82–90 mL/h, and slightly decreased to 72–80 mL/h in the presence of mesoporous Pd-Fe/SiO_2 microspheres. However, the water flow decreased to 58–70 mL/h when pure NZVI was packed in the column, depicting that mesoporous SiO_2 microspheres is a good support with good permeability to disperse ZVI for remediation of chlorinated compounds in porous media.

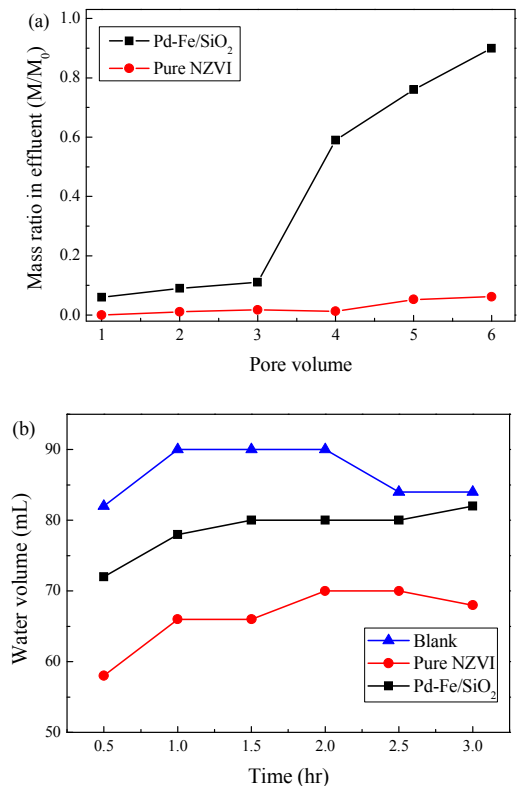

Fig. 8. (a) The breakthrough curves and (b) permeability of pure NZVI and mesoporous 0.5 wt% Pd-Fe/SiO_2 microspheres. M/M_0 represents the fraction of particles that are eluted in the effluent.

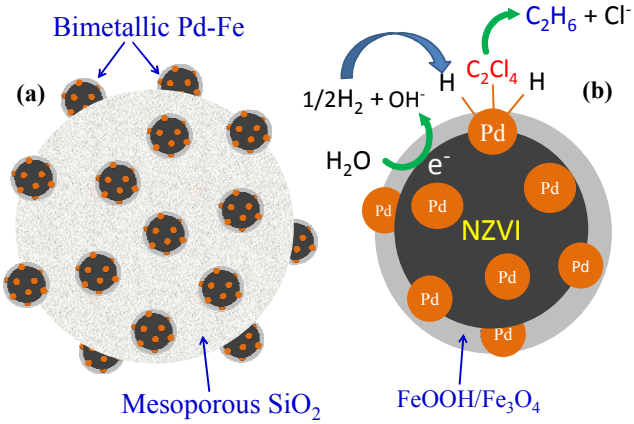

Fig. 9. The (a) immobilization of Pd-Fe nanoparticles onto mesoporous SiO_2 microspheres and (b) proposed mechanism for PCE dechlorination by mesoporous Pd-Fe/SiO_2 microspheres.

Fig. 9 shows the possible reaction mechanism for PCE dechlorination by mesoporous Pd-Fe/SiO_2 microspheres under anoxic conditions. The negatively changed silica surface can adsorb Fe^{2+} ions and then converted to NZVI in the presence of $NaBH_4$, which can be well dispersed onto the surface of SiO_2 microspheres to enhance the reactivity of Fe/SiO_2. The silica-supported Pd-Fe nanoparticles were electrochemically generated when Pd^{2+} ions were adsorbed onto the NZVI surfaces. The hydrodechlorination of PCE by bimetallic Pd−Fe nanoparticles involves the oxidation of NZVI to galvanically protect the Pd metal and Pd metals provide active sites for hydrodechlorination.[48] As the corrosion of NZVI increases, protons from water are reduced to adsorbed H atoms and to molecular hydrogen at the catalytic Pd surface, resulting in the formation of ethane during the hydrodechlorination of PCE.

4. Conclusions

In this study, we have first demonstrated the use of mesoporous SiO_2 microspheres as the support to well disperse the bimetallic Pd-Fe nanoparticles for hydrodechlorination of PCE under anoxic conditions. TEM images and surface area analysis showed that the poorly crystalline SiO_2 provided large specific surface areas for immobilization of Pd-Fe nanoparticles. The dechlorination reaction by Fe/SiO_2 followed pseudo-first-order reaction and Fe mass normalized rate constant of Fe/SiO_2 was 5.2 times higher than that of pure NZVI at pH 5.5. Addition of Pd ions enhanced the efficiency and dechlorination rate and the k_{obs} for PCE dechlorination by Fe/SiO_2 was significantly enhanced by 2–3 orders of magnitude after the addition of 0.5–3 wt% Pd ions. The Pd-Fe/SiO_2 microspheres showed excellent reusability toward PCE dechlorination which can be recycled for at least 10 times. The mesoporous silica plays an important role to immobilize and well disperse NZVI on surface, which can provide maximum numbers of active sites for dechlorination of PCE. Column experiments prove that mesoporous silica is a good carrier for bimetallic Pd-Fe nanoparticles to pass through the bed of glass beads and shows better permeability than that of bare NZVI. Results obtained in this study clearly indicate that the mesoporous Pd-Fe/SiO_2 microspheres are environmentally friendly composites for effective and efficient dechlorination of chlorinated hydrocarbons and can open an avenue to tailor mesoporous nanocomposites for long-term dechlorination of chlorinated compounds in porous media.

Acknowledgements

The authors thank Ministry of Science and Technology (MOST), Taiwan for financial support under grant No. NSC 101-2221-E-007-084-MY3.

Notes and references

1 D. Kaown, O. Shouakar-Stash, J. Yang, Y. Hyun, K. K. Lee, *Groundwater*, 2014, 52, 875-885.
2 M. Muchitsch, T. Van Nooten, L. Bastiaens, P. Kjeldsen, *J. Contam. Hydrol.*, 2011, 126, 258-270.
3 J. E.Cambers, M. H. Loke, R. D. Ogilvy, P. I. Meldrum, *J. Contam. Hydrol.,* 2004, 68, 1-22.
4 J. Koenig, M. Lee, M. Manefield, Rev. *Environ. Sci. Biotechnol.* 2015, 14, 49-71.
5 I. Bacsi, S. Gonda, V. B-Beres, Z. Novak, S. A. Nagy, G. Vasas, *Ecotoxicol.*, 2015, 24, 823-834.
6 J. Z. Zheng, Z. J. Xue, S. F. Li, S. X. Li, Z. M. Rao, *Anal. Methods*, 2012, 4, 2791-2796.
7 R. A. Doong, C. C. Lee, C. M. Lien, *Chemosphere*, 2014, 97, 54-63.
8 Y. Ma, X. M. Du, Y. Shi, Z. Xu, J. D. Fang, Z. Li, F. S. Li, *Chemosphere*, 2015, 121, 117-123.
9 R. A. Maithreepala, R. A. Doong, *Environ. Sci. Technol.*, 2005, 39, 4082-4090.
10 X. Liang, Y. Dong, T. Kuder, L. R. Krumholz, R. P. Philp, E. C. Bulter, *Environ. Sci. Technol.*, 2007, 41, 7094-7100.
11 C. C. Lee, R. A. Doong, *Appl. Catal. B: Environ.*, 2014, 144, 182-188.
12 F. L. Fu, D. D. Dionysiou, H. Liu, *J. Hazard. Mater.*, 2014, 267, 194-205.
13 C. C. Huang, H. L. Lien, *Water Sci. Technol.*, 2010, 62, 202-208.
14 G. K., Parshetti, R. A. Doong, *Chemosphere*, 2012, 86, 392-399
15 N. C. Mueller, J. Braun, J. Bruns, M. Černík, P. Rissing, D. Rickerby, B. Nowack, *Environ. Sci. Pollut. Res.*, 2012, 19, 550–558.
16 W. Yan, H. L. Lien, B. E. Koelc, W. X. Zhang. *Environ. Sci.: Process Impacts*, 2013, 15, 63-77.
17 Y. H., Shih, M.Y., Chen, Y. F. Su, *Appl. Catal. B Environ.*, 2011, 105, 24-29.
18 H. L, Lien, W. X. Zhang, *Appl. Catal. B. Environ.*, 2007, 77, 110-116.
19 R. A., Doong, Y. L. Lai, Chemosphere, 2006, 64, 371-378.
20 F. He, D. Y., Zhao, C. Paul, Water Res., 2010, 44, 2360–2370.
21 P. Jiemvarangkul, W.X. Zhang, H.-L. Lien. *Chem. Eng. J.*, 2011,170 482–491.
22 C. M. Kocur, A. I. Chowdhury, N. Sakulchaicharoen, H. K. Boparai, K. P. Weber, P. Sharma, M. M. Krol, L. Austrins, C. Peace, B. E. Sleep, D. M. O'Carroll, *Environ. Sci. Technol.*, 2014, 48, 2862-2869.
23 H. Ma, Y. P. Huang, M. W. Shen, R. Guo, X. Y. Cao, X. Y. Shi, *J. Hazard. Mater.*, 2012, 11-212, 349-356.
24 F. He, D. Y. Zhao, *Environ. Sci. Technol.*, 2007, 41, 6216–6221.
25 B. Schrick, B. W. Hydutsky, J. L. Blough, T. E. Mallouk, *Chem. Mater.,* 2004, 16, 2187-2193.
26 V. Smuleac, R. Varma, S. Sikdar, D. Bhattacharyya, *J. Membrane Sci.*, 2011, 379, 131-137.
27 Y. F. Su, T. L. Cheng, Y. S. Shih, *J. Environ. Manage.*, 2013, 129, 361-366.
28 G. K. Parshetti, R. A. Doong, Water Res., 2009, 43, 3086-3094.
29 S. X. Li, J. Z. Zheng, D. J. Chen, Y. J. Wu, W. X. Zhang, F. Y. Zheng, J. Cao, H. Ma, Y. L. Liu, *Nanoscale*, 2013, 5, 11718-11724.
30 C. H. Tan, W. X. Zhang, J. Z. Zheng, X. L. You, X. A. Lin, S. Z. Li, *J. Mater. Chem. B.*, 2015, 3, 7117-7124.
31 W. X. Xhang, J. Z. Zheng, X. H. Tan, C. H. Tan, X. A. Lin, S. R. Hu, J. H. Chen, X. L. You, S. X. Li, *J. Mater. Chem. B*, 2015, 3, 217-224.
32 Y. Y. Xie, Z. Q. Fang, X. H. Qiu, E. P. K. Tsang, B. Liang, Chemosphere, 2014, 108 433-436.
33 L. M. Kustov, S. R. Al-Abed, J. Virkutyte, O. A. Kirichenko, E. V. Shuvalova, G. I. Kapustin, I. V. Mishin, V. D. Nissenbaum, O. P. Tkachenko, E. D. Finashina, *Pure Appl. Chem.*, 2014, 86, 1141-1158.

34 B. Ensie, S. Samad, *Desalination*, 2014, 347, 1-9.
35 P. X. Wu, C. M. Liu, Z. J. Huang, W. M. Wang. *RSC Adv.*, 2014, 4, 25580-25587.
36 Q. Cai, Z. S. Luo, W. Q. Pang, Y. W. Fan, Z. H. Chen, F. Z. Cui. *Chem. Mater.*, 2001, 13, 258-263.
37 L. Yang, L. Lv, S. Zhang, B. Pan, W. Zhang, *Chem. Eng. J.*, 2011, 178, 161-167.
38 G. K. Parshetti, R. A. Doong, Water Res., 2011, 45, 4198-4210.
39 Y. H. Tee, E. Grulke, D. Bhattacharyya, *Ind. Eng. Chem. Res.*, 2005, 44, 7062-7070.
40 C. C. Lee, R. A. Doong, *Environ. Sci. Technol.*, 2008, 42, 4752-4757.
41 C. J. Lin, S. L. Lo, Y.H. Liou, *J. Hazard. Mater.*, 2004, 116, 219-228.
42 C. A. González; C. M. de Correa. *Ind. Eng. Chem. Res.*, 2010, 49, 490–497.
43 S. Pitkaaho, L. Matejova, S. Ojala, J. Gaalova, R. L. Keiski, *Appl. Catal. B Environ.*, 2012, 113-114, 150-159.
44 R. F. Bueres, E. Asedegbega-Nieto, E. Díaz, S. Ordóñez, F. V. Díez, *Catal. Today*, 2010, 150, 16–21.
45 V. Nagpal, A. D. Bokare, R. C. Chikate, C. V. Rode, K. M. Paknikar, *J. Hazard. Mater*., 2010, 175, 680-687.
46 E. J. eardon, R. Fagan. J. L. Vogan, A. Przepiora, *Environ. Sci. Technol*., 2008, 42, 2420-2425.
47 J. J. Zhan, T. H. Zheng, G. Piringer, C. Day, G. L. McPherson, Y. F. Lu, K. Papadopoulos, V. T. John, *Environ. Sci. Technol.*, 2008, 42, 4494-4499.
48 S. J. Li, Y. L. Fang, C. D. Romanczuk, Z. H. Jin, T. L. Li, M. S. Wong. *Appl. Catal. B. Environ.*, 2012, 25, 95-102.